ACS Catalysis

pubs.acs.org/acscatalysis

Research Article

Differences in Mechanism and Rate of Zeolite-Catalyzed Cyclohexanol Dehydration in Apolar and Aqueous Phase

Feng Chen, Manish Shetty, Meng Wang, Hui Shi,* Yuanshuai Liu, Donald M. Camaioni, Oliver Y. Gutiérrez, and Johannes A. Lercher*

Cite This: *ACS Catal.* 2021, 11, 2879−2888

Read Online

ACCESS | Metrics & More | Article Recommendations | Supporting Information

ABSTRACT: The rate of acid−base-catalyzed dehydration of alcohols strongly depends on the solvent and the environment of the acid sites. We find that Brønsted acidic sites in large-pore zeolites, but not in medium-pore zeolites, catalyze cyclohexanol dehydration in decalin at significantly higher rates than hydrated hydronium ions in aqueous phase. Specifically, the difference in turnover rates between the two solvents amounts to 2−3 orders of magnitude on H-BEA and H-FAU, while being very modest (within a factor of 2) for H-MFI. Combining kinetic, isotopic tracer, and ^{2}H NMR measurements, it is established that cyclohexanol dehydration generally follows an E1-elimination pathway in decalin. A notable exception is the monomer dehydration route on H-MFI, which exhibits a much lower activation energy and a substantially negative activation entropy that appear to be associated with an E2-type mechanism. The C−O bond cleavage displays a dominant degree of rate control in decalin, which stands in contrast to deprotonation (C−H cleavage) being rate-limiting in aqueous-phase dehydration.

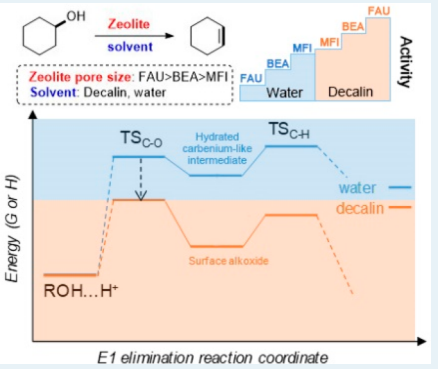

KEYWORDS: *alcohol dehydration, solid−liquid interface, confinement effect, zeolites, elimination mechanism*

1. INTRODUCTION

Acid-catalyzed reactions in the liquid phase are central to many synthetic strategies and have become central in the context of upgrading biomass-derived oxygenates into liquid fuels and chemicals.[1−11] Considering the wide application of these reactions, it seems surprising that the mechanisms of acid−base catalysis at solid−liquid interfaces are not well understood at an elementary level. This is related to challenges in elucidating the fundamental structure−function relations at solid−liquid interfaces,[12−20] including the solvation of the reacting substrates, their interactions with the catalyst, the dynamic nature of the active sites, and subtle variations in the reaction pathways.[15]

Solvents bring about another layer of complexity because of intra- and intermolecular interactions (e.g., dipolar, electrostatic, H-bonding) that influence not only the nature of active sites but also the stability of intermediates and transition states along a reaction pathway.[21−23] In the presence of even modest chemical potentials of water, the acidic proton of the zeolite framework is transformed to a hydrated hydronium ion.[24] We recently discovered that these hydronium ions confined largely inside zeolite pores lead to up to 2 orders of magnitude higher dehydration rates of cyclohexanol compared with rates measured in acidic aqueous solutions.[25,26] Dumesic and co-workers showed that the stabilization of the acidic proton relative to the positively charged transition states determines the rates of acid-catalyzed reactions of hydroxyl-containing compounds. This often leads to substantial rate enhancements compared to pure water for both homogeneous and solid acids in the presence of polar aprotic solvents and their mixtures with water.[21−23]

In order to understand these effects, this work aims to provide a benchmark for liquid-phase alcohol dehydration in the absence of strong solvent interactions.[27−36] Having reported how nanoscopic confinement induced by zeolite pores affects the dehydration rates in water,[25] we investigate in this study how dehydration catalysis is impacted by such pore constraints in the apolar solvent decalin, which was found to dissolve the alcohol more readily than the linear hydrocarbons and therefore allowed for a wider range of alcohol concentrations to be accessed for kinetic studies. Furthering our previous work[37,38] focused on a single zeolite (H-BEA with Si/Al = 75), we report herein thermochemical and kinetic measurements in conjunction with isotope labeling, to elucidate the reaction mechanism of cyclohexanol dehydration in decalin, to quantitatively assess the influence of steric environment on the reactivity of Brønsted acid sites without

Received: December 25, 2020
Revised: February 3, 2021
Published: February 17, 2021

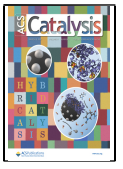

https://dx.doi.org/10.1021/acscatal.0c05674
ACS Catal. 2021, 11, 2879−2888

complete water solvation, and to contrast with alcohol dehydration previously reported for aqueous media.[25,26] The results show a significantly different manifestation of confinement effects than that observed for aqueous-phase dehydration, which primarily results from the stabilities and, thus, the relative surface concentrations of alcohol-derived intermediates and kinetically relevant transition states that have divergent sizes and polarities.

2. RESULTS AND DISCUSSION

2.1. Kinetics of Zeolite-Catalyzed Cyclohexanol Dehydration in Decalin. The present work compares three framework types with distinct pore topologies, namely, FAU, BEA, and MFI (implicitly in their H-forms), which have been previously investigated for the aqueous-phase dehydration of cyclohexanol.[25,26] In decalin, the dehydration of cyclohexanol leads to cyclohexene as the dominant product (selectivity: 95−100%) on all zeolites. A minor product, dicyclohexyl ether, was detected only on the large-pore zeolites, BEA and FAU (Figure S1; 0.33 M alcohol, 413 K). The initial rates on zeolites, assessed at conversions of 5−20%, were normalized to the concentrations of Brønsted acid sites (BAS).

Before discussing rate data, we first briefly address the chemical state of the acid sites. In the case of MFI, according to the estimated maximum vapor pressure of water in the reactor and the water adsorption isotherms reported earlier,[39] the initial state of the BAS is a framework-bound proton at a bridging Si−OH−Al group. At increased alcohol conversions, the amount of water formed potentially changes the localized BAS to a hydronium ion. It can be also estimated, however, that the equilibrium size of hydronium ions during the dehydration of cyclohexanol in decalin remains substantially smaller than in the aqueous phase, where $H(H_2O)_{7-8}^+$ is the most probable form of intrapore hydronium ions in MFI. Detailed discussions regarding the state of BAS in the presence of intraporous decalin, alcohol, and water are presented in Section 5 of the Supporting Information (SI).

Rate data on BEA, MFI, and FAU zeolites with varying Si/Al ratios are summarized in Supplementary Figure S1 (0.33 M alcohol in decalin, 413 K). For each framework type, varying the Si/Al ratio resulted in up to a factor of 3 variations in the turnover frequency (TOF, based on BAS concentrations) of cyclohexanol dehydration. Without the formation of hydronium ions in the pore, this rate dependence on the Si/Al ratio may be attributed to different crystallographic and topological locations of framework Al and the associated protons, as well as to constraints in the zeolite pores induced by extraframework Al debris. If decalin, cyclohexanol and hydronium ions coexist in the zeolite pores (SI, Section 5), it is plausible that such rate changes are induced by the varied polar environments that would affect the stability of charged intermediates and transition states involved in alcohol dehydration. In the spirit of focusing on the elucidation of reaction mechanism and the impact of steric confines on kinetic parameters, catalysts with the highest TOF for each framework type, that is, FAU (Si/Al = 30), BEA (Si/Al = 75), and MFI (Si/Al = 40), were chosen for further studies; the physicochemical properties of these materials are shown in Supplementary Table S1. It is important to mention that the concentration of Lewis acid sites was relatively low (<50 μmol g^{-1}) in all three samples.

The TOFs for cyclohexene formation, at an alcohol concentration of 0.33 M in decalin (Figure 1), increased with increasing pore dimensions (MFI: 0.51 × 0.55 nm and 0.53 × 0.56 nm, BEA: 0.66 × 0.67 nm and 0.56 × 0.58 nm, FAU: 0.74 × 0.74 nm), in an apparent reversed order compared with the trend for aqueous-phase dehydration of the same molecule.[25,26] For BEA and FAU, the reaction proceeded at rates ∼50 to ∼800 times faster in decalin than in water, whereas for MFI, the TOF in decalin was comparable (within a factor of 2) to that in aqueous phase.[25,26]

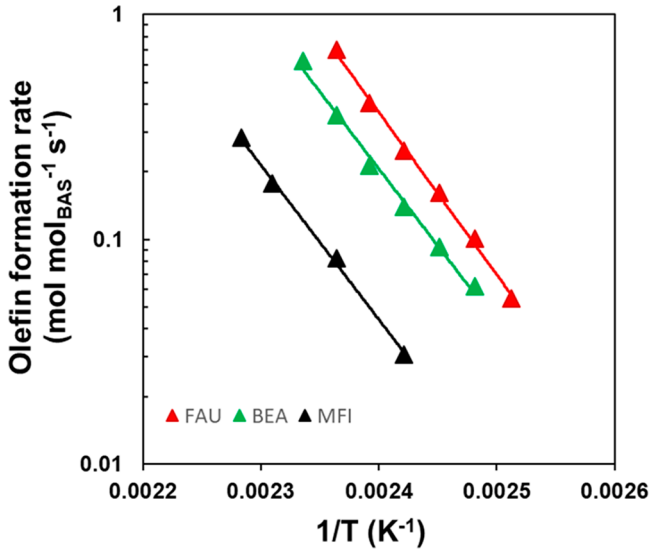

Figure 1. Measured turnover frequencies (TOFs) of cyclohexene formation from dehydration of cyclohexanol (0.33 M in decalin) with different zeolites: FAU (Si/Al = 30), BEA (Si/Al = 75), and MFI (Si/Al = 40). Rates were determined at conversions <20%. Solid lines are fits to the Arrhenius equation. Turnover numbers (TONs) were all much larger than 10, demonstrating the catalytic nature of the reaction.

2.2. On the Mechanism of Cyclohexanol Dehydration in Decalin over Zeolites. For all zeolites, cyclohexanol dehydration rates exhibited zero-order dependence with respect to cyclohexanol (>0.1 M) in aqueous phase.[25] In contrast, dehydration rates in decalin decreased with increasing concentration of cyclohexanol (0.025−1.0 M) for these zeolites (Figure 2). This trend resembles the gas-phase alcohol dehydration catalyzed by zeolites[40,41] and polyoxometalate clusters.[42−45] In the gas phase, this has been attributed to the coverage of active sites by unreactive or much less reactive alcohol−alcohol dimers with increasing alcohol pressure.[41] As decalin is an apolar and only weakly interacting solvent, we hypothesize that the intramolecular dehydration of cyclohexanol to cyclohexene occurs via monomer- and dimer-mediated routes on acidic zeolites in decalin, analogous to gas-phase alcohol dehydration on solid Brønsted acids.[41] The dimer route is much slower than the monomer route, as previously shown.[37,38] Note, however, that the magnitude of the decrease in rates at 413 K with increasing alcohol concentration is the smallest on MFI and the greatest on FAU, reflecting the combined effects of coverages and reactivities of monomer and dimer species in zeolites of different confining environments. At higher temperatures (e.g., 443 K), the rates on MFI depended only weakly on the alcohol concentration, the cause of which is analyzed later on the basis of kinetic fitting (Section 2.3).

To investigate the reaction mechanism in decalin, H/D isotope tracer studies were used in conjunction with ^{2}H NMR experiments. The dehydration of 1-D-cyclohexanol was carried

https://dx.doi.org/10.1021/acscatal.0c05674
ACS Catal. 2021, 11, 2879−2888

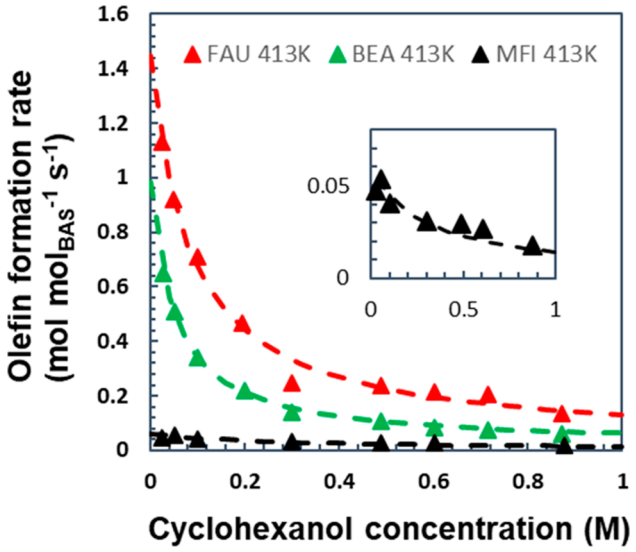

Figure 2. TOFs for cyclohexanol dehydration in decalin on different zeolites as a function of cyclohexanol concentration. The inset shows an enlarged view of the rate data on MFI. Reaction conditions: 0.025−0.90 M (r.t.) cyclohexanol in decalin, 413 K. Rates were determined at conversions of <20%.

out on zeolites in decalin, and the products were analyzed with ^{2}H NMR at varying conversions and concentrations of cyclohexanol. 1-D-Cyclohexene and 3-D-cyclohexene were both detected, while the signal of 4-D-cyclohexene overlapped with that of decalin (nonlabeled) and, thus, was not quantified reliably. 1-D-Cyclohexene may be generated from 1-D-cyclohexanol dehydration via both E1 and E2 elimination pathways. Along the E1 pathway, 3-D- and 4-D-cyclohexenes would form through 1,2-hydride shifts of carbenium ions following the cleavage of the C−O bond in 1-D-cyclohexanol (Scheme 1). Along the E2 pathway, 3-D- and 4-D-isotopomers would not form directly from the dehydration of 1-D-cyclohexanol; instead, they would form via secondary reactions (readsorption, protonation, and label shifts) of 1-D-cyclohexene.

Deuterium label shifts were observed in the reactions of 1-D-cyclohexanol catalyzed by FAU, BEA, and MFI (Figure 3 and

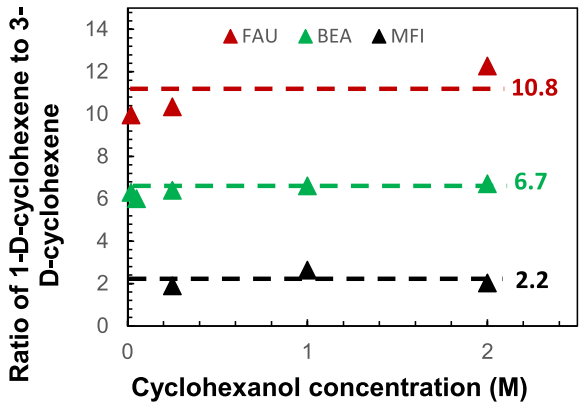

Figure 3. Ratio of 1-D-cyclohexene to 3-D-cyclohexene from 1-D-cyclohexanol dehydration with FAU, BEA, and MFI in decalin up to alcohol conversions of 20%.

Supplementary Figures S6−S11). For example, the ratio of 1-D-cyclohexene to 3-D-cyclohexene remained relatively constant (6.7 on average) as the reaction proceeded on BEA until secondary reactions involving olefin readsorption and proto-

Scheme 1. Possible Reaction Pathways (E1 and E2 Elimination) for 1-D-Cyclohexanol Dehydration

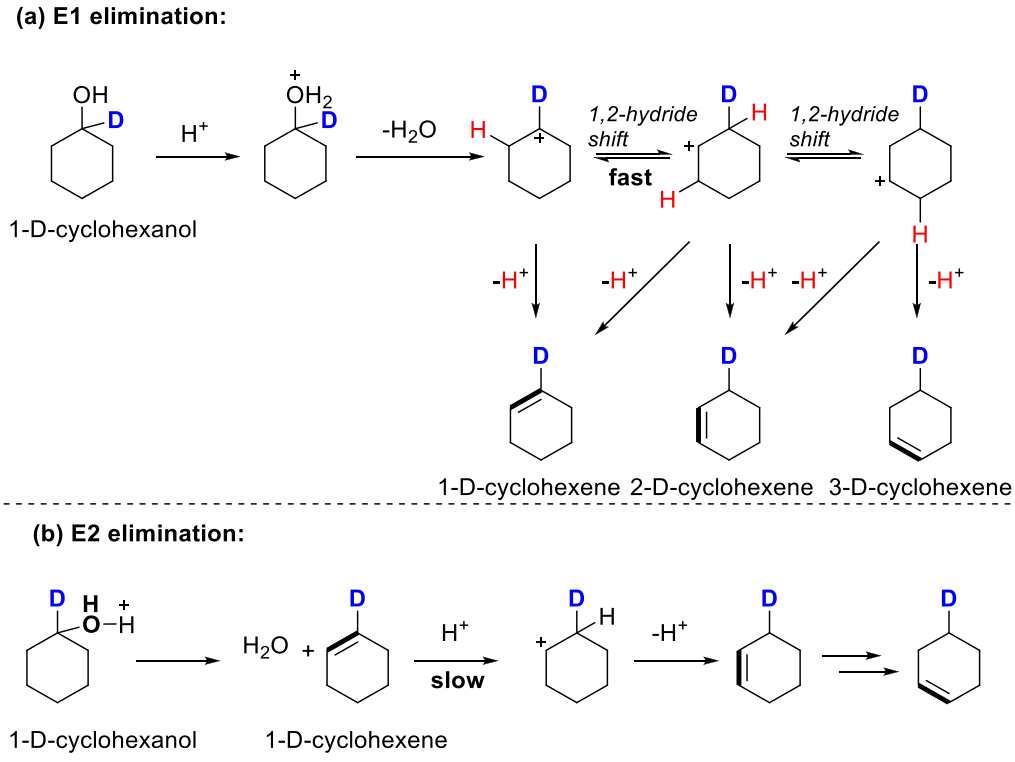

https://dx.doi.org/10.1021/acscatal.0c05674
ACS Catal. 2021, 11, 2879−2888

nation set in at high conversions (Supplementary Figure S6). The presence of these label-shifted olefin isotopomers even at low conversions suggests that a major portion of cyclohexanol dehydration passes through a carbenium ion-type intermediate following an E1 elimination pathway, though it remains difficult to fully exclude that label shifts occur while the olefin diffuses out of the pores and interacts with protons along the diffusion path.

With BEA, the ratio of 1-D-cyclohexene to 3-D-cyclohexene (measured at alcohol conversions up to 20% in most cases) did not change with the alcohol concentration from 0.02 to 2.0 M and was only slightly smaller than that observed for the dehydration of neat cyclohexanol (ca. 9.6 M; Supplementary Figure S6). Interestingly, however, the ratio of 1-D-cyclohexene to 3-D-cyclohexene was 1.9−2.6 for MFI and 10−14 for FAU (Figure 3). While we attribute this to a better stabilization of the transition state for 1,2-hydride shifts in the medium-pore zeolite (MFI) than in larger pores, we cannot fully exclude that olefin readsorption and protonation at the BAS and the ensuing hydride shifts occurs with higher rates along the pore-exiting path of the olefin product in MFI. Taken together, we conclude that the elimination of cyclohexanol displays a dominant E1 character across the studied range of alcohol concentration (0.02−2.0 M) in decalin, while we caution that the experiments do not provide a stringent mechanistic proof for the complete absence of an E2-elimination path.

The proposed sequence for cyclohexanol dehydration catalyzed by zeolites in decalin (Scheme 2) illustrates that for the monomer route, the elimination generally occurs stepwise. Specifically, cyclohexanol first adsorbs on a BAS to form cyclohexanol monomer (Step 1). The cleavage of the C−O bond of the monomer produces a surface-bound carbenium ion-type intermediate, likely a surface alkoxy group in the absence of significant concentrations of water (Step 2). Finally, deprotonation (i.e., C−H bond cleavage) of the intermediate leads to the formation of cyclohexene, which desorbs to regenerate the BAS (Step 3). A protonated dimer is hypothesized to be generated through the interaction of the formed monomer with another cyclohexanol (Step 4). This dimer species potentially also converts to the alkene (e.g., via Step 5 that is not necessarily an elementary step), which is energetically more demanding and, hence, slower than the monomer route according to recent density functional theory (DFT) calculations of 1-butanol[46−48] and 1-propanol[41] dehydration in zeolites and our earlier measurements in gas-phase alcohol conversions.[17] Some prior literature even treated dimers as unreactive species.[14,43,41]

Scheme 2. Proposed Sequence of Key Reaction Steps in Cyclohexanol Dehydration (in Gas Phase or in Decalin) with the Relevant Kinetic and Thermodynamic Coefficients Denoted

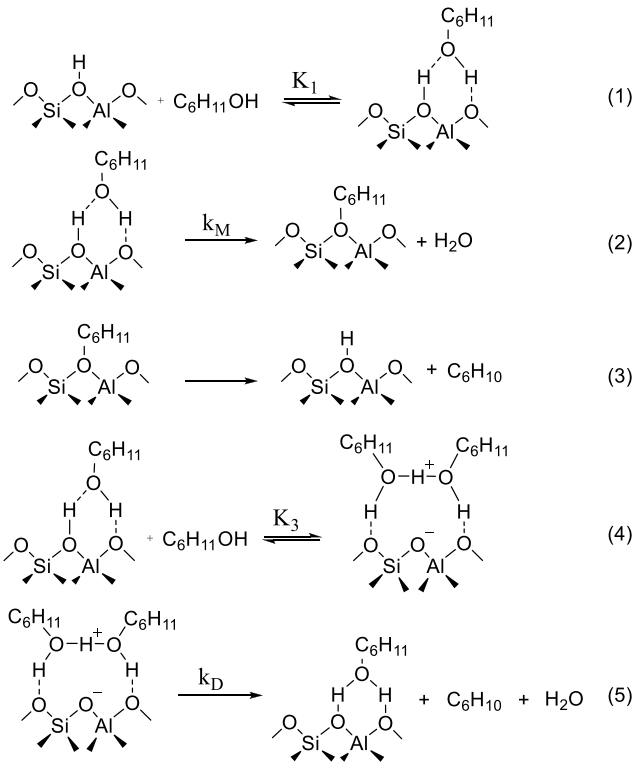

Along the E1 elimination path, either C−O or C−H bond cleavage is the rate-determining step (RDS), or in other words, one of the two steps has a greater degree of rate control.[45−47] This question was probed by measuring kinetic H/D isotope effects (KIEs) for cyclohexanol dehydration on the three zeolites. In one set of experiments (only performed on BEA), the TOFs of olefin formation from cyclohexanol-d_{12} and 1-D-cyclohexanol were measured at 403 K (Supplementary Table S6). The KIE for the pair of cyclohexanol-d_0 and cyclohexanol-d_{12} (i.e., $TOF_{C_6H_{11}OH}/TOF_{C_6D_{11}OD}$) was 1.58 and 1.42, while for the pair of cyclohexanol-d_0 and 1-D-cyclohexanol, the KIE was 1.42 and 1.19, at alcohol concentrations of 0.025 and 0.1 M, respectively. In another set of experiments, a mixture of cyclohexanol-d_0 and cyclohexanol-d_{12} was reacted on the three zeolites (50 mol % of each substrate with a total concentration of 0.025 M solution at 413 K, that is, each at 0.0125 M). The initial molar ratio of cyclohexene-d_0 to cyclohexene-d_{10}, also representing a KIE, varied from 1.79:1 to 2.15:1 on the three zeolites (Supplementary Table S7). Because the measured KIEs are based on rate ratios, rather than ratios of rate constants, the increase in the measured KIE (which contains contributions from KIEs for both monomer and dimer routes, weighted by the individual coverages of the monomer and dimer species) with decreasing alcohol concentration points to higher intrinsic KIEs (∼2) associated with the monomer-mediated elimination path.

At these temperatures, rehybridization of α-C_{sp^3} (in a protonated alcohol monomer species) to α-C_{sp^2} (resembling the TS) would lead to secondary KIE values (1.2−1.4) for C−O bond cleavage as the RDS. Thus, the measured KIEs indicate that the C−O bond cleavage exerts a higher degree of rate control than the C−H cleavage for cyclohexanol dehydration in decalin. This is in contrast to the same reaction occurring in aqueous phase where the C−H bond cleavage shows a dominant degree of rate control, displaying primary KIEs of 2.9−3.5 that are close to the theoretical maximum for a late TS of C−H cleavage.[26]

The somewhat larger KIEs than the values expected solely from rehybridization of the α-carbon in the C−O cleavage step in the formation of carbenium ion might indicate a small degree of rate control by the C−H bond cleavage step.[26] By the same token, the decrease in KIE with increasing alcohol concentration suggests a greater degree of rate control by the C−O cleavage step along the dimer dehydration route

https://dx.doi.org/10.1021/acscatal.0c05674
ACS Catal. 2021, 11, 2879−2888

compared with the monomer route, as expected from the larger coverage of cyclohexanol dimers at higher concentrations (section 2.3). Thus, we deduce that cyclohexanol dehydration in decalin (an apolar medium) proceeds primarily via E1 elimination on the zeolites, with the highest degree of rate control exerted by the C−O cleavage step. This (tentative) conclusion is further analyzed using activation enthalpies and entropies.

2.3. Impact of Pore Constraints on the Rate Constants and Activation Parameters. On the basis of the proposed sequence of steps in Scheme 2, the following expression for the TOFs (eq 1), is derived, which captures the contribution from monomer- and dimer-mediated pathways for olefin formation (detailed derivations in the SI):

$$\frac{r_{olefin}}{[H^+]_0} = TOF = \frac{k_M K_1 [C_6H_{11}OH] + k_D K_1 K_3 [C_6H_{11}OH]^2}{1 + K_1 [C_6H_{11}OH] + K_1 K_3 [C_6H_{11}OH]^2} \quad (1)$$

in which the kinetic and thermodynamic constants carry the meanings as indicated in Scheme 2: specifically, k_M and k_D are the intrinsic rate constants for the monomer- and dimer-elimination steps, respectively; K_1 is the equilibrium constant for alcohol monomer formation from the BAS and an alcohol in the liquid phase; K_3 is the equilibrium constant for alcohol dimer formation from a H-bonded monomer at the BAS and an alcohol in the liquid phase; $[H^+]_0$ is the total concentration of BAS.

When the latter two terms in the denominator of eq 1 dominate, the dependence of the TOF on cyclohexanol concentration is approximated by eq 2:

$$TOF = \frac{k_M + k_D K_3 [C_6H_{11}OH]}{1 + K_3 [C_6H_{11}OH]} \quad (2)$$

Consequently, the kinetic parameters for cyclohexanol dehydration on the three zeolites in decalin were obtained by fitting the kinetic data obtained at 413 K (Figure 2) to eq 2 (Table 1). To reduce the degrees of freedom in fitting the data as well as to increase the precision in fitted values for k_M and K_3, k_D was constrained to values that reproduce the measured TOF for cyclohexene formation in neat cyclohexanol (assuming a complete coverage by cyclohexanol dimers at concentration of ∼9.6 M). The term $[C_6H_{11}OH]$ refers to the thermodynamic activity of alcohol rather than its concentration in decalin (an extended discussion of this matter is presented in Section 3 of the SI). Note also that the derivations of eqs 1 and 2 do not require that E1 elimination be the sole dehydration mechanism; assumptions of a series of steps along a concerted E2 path would lead to the same rate expressions, albeit with somewhat different meanings assigned to the rate constants.

Table 1. Intrinsic Rate Constants (Normalized to the BAS Concentration) for the Formation of Cyclohexene from Cyclohexanol by Monomer- and Dimer-Mediated Dehydration Routes and the Monomer-Dimer Equilibrium Constant over Zeolites FAU, BEA, and MFI in Decalin at 413 K[a]

zeolite	k_M (s^{-1})	k_D (s^{-1})	k_M/k_D	K_3 (M^{-1})
FAU	1.744 ± 0.107	0.058	30.0	18.6 ± 2.5
BEA	1.010 ± 0.041	0.023	43.9	23.5 ± 1.9
MFI	0.052 ± 0.004	0.006	8.7	2.9 ± 0.7

[a] k_M and k_D are the intrinsic rate constants for the monomer- and dimer-mediated dehydration pathways, respectively. In practice, k_D was always set to give the measured TOF of cyclohexene formation in the neat phase (100% cyclohexanol, 9.6 M). K_3 is the equilibrium constant for alcohol dimer formation from a monomer and an alcohol in the liquid phase.

The rate constants, obtained by regression, for both monomer- and dimer-mediated dehydration routes increase with the increase in pore dimensions from MFI to FAU, following the same trends observed for TOFs at any given concentration. The contribution from the monomer pathway for dehydration decreases with increasing cyclohexanol concentration. The rate constant for the monomer pathway is 30−44 times greater than that for the dimer pathway on the two large-pore zeolites, whereas the difference in monomer-path rate constant is much smaller (∼9 times) on MFI. As a result, at the lowest concentration studied here (∼0.02 M), the ratio of the rates along the monomer and dimer routes is 80−90 on FAU and BEA and ∼150 on MFI. This ratio becomes unity, that is, equal contributions by the monomer and dimer routes, at ∼1.5−2.0 M of cyclohexanol. For the dehydration of neat alcohol (9.6 M), this ratio would drop to 0.1−0.2, showing the preponderance of the dimer route.

Using the same protocol, k_M and K_3 were derived (k_D being fixed to give the TOF of neat alcohol dehydration) from rate-concentration data acquired at temperatures in the ranges 403−433 K for BEA and FAU and 413−443 K for MFI. Table 2 compiles enthalpies and entropies of activation obtained from the Eyring plots of rate constants, k_M and k_D, as well as free energies of activation calculated for the regressed intrinsic rate constants on the three zeolites at 423 K. Interestingly, activation enthalpies and entropies for monomer and dimer dehydrations were comparable on the two large-pore zeolites, FAU and BEA. MFI appears to be quite different, showing a much lower activation enthalpy and a negative activation entropy for the monomer route but a much higher activation enthalpy and a positive activation entropy for the dimer route.

Conceptually, the negative entropy of activation for the monomer route on MFI is an indication for an E2-elimination path, which appears, at first sight, to contradict our foregoing mechanistic analysis. We surmise that the observed label shifts on MFI (^{2}H NMR; measured in an alcohol concentration range of 0.25−2.0 M) may not reflect the intrinsic characteristics of the monomer route and could be understood in terms of readsorption, protonation, and hydride shifts before exiting the pore. Adsorption of decalin (cross section: 0.70 × 0.52 nm) is significantly impeded in MFI, with its vapor-phase saturation uptake accounting for only 10% of the micropore volume, suggesting low diffusion rates of decalin and similarly sized molecules in MFI pores (sinusoidal channels: 0.51 × 0.55 nm and straight channels: 0.53 × 0.56 nm). As a consequence, van der Waals stabilizations provided by decalin are lacking for the monomer route in MFI, unlike the other two large-pore zeolites that allow decalin to coadsorb in the pore. In this case, a stepwise pathway is hypothesized to be unfavorable on MFI because of the lack of coadsorbed species that assist in the stabilization of charged TS. For the aqueous-phase dehydration, the pore is fully occupied by water and alcohol molecules that are more effective in stabilizing charged intermediates and transition states. Hence, an E1-type mechanism was concluded to be dominating for the aqueous-phase dehydration of cyclohexanol on all zeolites.[25,26]

https://dx.doi.org/10.1021/acscatal.0c05674
ACS Catal. 2021, 11, 2879−2888

Table 2. Intrinsic Activation Parameters for Dehydration of Cyclohexanol in Decalin with the Chosen Zeolites[a]

	$\Delta H^{o\ddagger}$ (kJ mol^{-1})		$\Delta S^{o\ddagger}$ (J K^{-1} mol^{-1})		$\Delta G^{o\ddagger}_{423\ K}$ (kJ mol^{-1})	
zeolite	monomer	dimer	monomer	dimer	monomer	dimer
FAU	127 ± 4	119 ± 1	60 ± 9	16 ± 1	102 ± 1	111 ± 1
BEA	130 ± 7	120 ± 11	68 ± 16	11 ± 1	101 ± 1	114 ± 1
MFI	76 ± 6	194 ± 15	−88 ± 14	176 ± 14	113 ± 1	119 ± 1

[a]The error bars for $\Delta H^{o\ddagger}$ and $\Delta S^{o\ddagger}$ represent the 1-σ standard deviations.

Note that using eq 1 (that accounts for low BAS coverage regime) to fit the rate data, a different set of regressed rate and equilibrium constants would be found. In this approach, to reduce the degrees of freedom in the fitting procedure, k_D was again set to reproduce the TOF of neat alcohol dehydration and additionally, K_1 (i.e., adsorption of an alcohol molecule from the decalin solution to form a H-bonded monomer on BAS) was obtained from independent calorimetric and adsorption measurements at room temperature and extrapolation to reaction conditions, while k_M and K_3 were regressed (discussed in Section 3 of the SI). As exemplified for MFI (cf. Table S3 and Table S5), using the complete rate eq (eq 1), the regressed rate constant for the monomer route (k_M) would increase by a factor of 2−3 compared to that obtained from the previous fitting protocol. Regardless, the conclusion does not change that rate constants (both k_M and k_D) on MFI are much smaller than those on FAU and BEA. For the activation enthalpies and entropies, the difference between the two fitting approaches is not substantial (cf. Table 2 and Table S4); in both cases, relatively low activation enthalpy and negative activation entropy—the hallmark of E2-elimination—were determined for the monomer route on MFI, as opposed to the other two zeolites.

2.4. Cyclohexanol Dehydration: A Tale of Two Solvents. In both water and decalin, we have demonstrated that cyclohexanol dehydration follows an E1 elimination path at the prevalent reaction conditions, with the only exception being the monomer route on MFI that seems to exhibit a pronounced E2-character. However, the rate constants in water and in decalin are associated with different rate-determining steps. In water, the C_α−O recombination is considerably faster than deprotonation (C_β−H cleavage) such that the latter step is rate-determining[25,26] (or, according to Campbell, this step has the highest degree of rate control[49−51]). In the presence of low thermodynamic activities of intraporous water, as is the case for gas-phase dehydration and in decalin, the deprotonation of the alkoxy intermediate by framework oxygen (a base) occurs at a rate sufficiently faster than that of C−O recombination. Under these conditions, C−O recombination occurs infrequently, at least because there are few water molecules present to reform the C−O bond. In this case ($r_{C-O\ recombination} \ll r_{deprotonation}$), C−O bond cleavage becomes the rate-determining step (see more detailed discussions in Section 4 of SI). Thus, the measured rate constant of aqueous-phase dehydration reflects the Gibbs free energy of the deprotonation TS relative to that of the associated complex of alcohol and hydrated hydronium ions, whereas the rate constants (for monomer- and dimer routes) of dehydration in decalin reflect the Gibbs free energy difference between the H_2O-elimination TS (i.e., C−O cleavage) and the respective adsorbed state (i.e., H-bonded monomer or protonated dimer).

The above understanding of the mechanism facilitates the interpretation of the observed differences in the rate constants and activation parameters for dehydration in water and in decalin. In the cases of BEA and FAU, the rate constants were more than 2 orders of magnitude smaller for aqueous-phase dehydration than the rate constants for monomer elimination route in decalin. Our earlier study demonstrated that the C−O cleavage/recombination TS lies at a Gibbs free energy close to or slightly lower than (by ∼5 kJ mol^{-1} at most) that of the C−H cleavage TS for aqueous-phase cyclohexanol dehydration in zeolites.[25] As a result, the rate constant for aqueous-phase dehydration corresponds to the free energy barrier of C−H cleavage and almost also reflects that of the C−O bond cleavage. In turn, we consider the measured free energies of activation to primarily reflect the difference in the free energy barrier for C−O cleavage between aqueous-phase and decalin-phase dehydration of cyclohexanol ($\Delta\Delta G^{\ddagger}_{C-O,\ water-decalin}$): specifically, the differences in the free energies of activation in water and in decalin are estimated from the respective rate constants to be ∼21−27 kJ mol^{-1} for FAU and BEA at 423 K (i.e., $\Delta G^{\ddagger}_{C-O,\ decalin}$ = 101−102 kJ mol^{-1}; $\Delta G^{\ddagger}_{C-O,\ water}$ = ∼122−129 kJ mol^{-1} at 423 K). A closer inspection indicates that such differences for both zeolites stem primarily from different activation enthalpies (∼159 and 166 kJ mol^{-1} in water vs 130 and 127 kJ mol^{-1} in decalin for BEA and FAU, respectively, i.e., $\Delta\Delta H^{\ddagger}_{C-O,\ water-decalin}$ = ∼29−39 kJ mol^{-1} for BEA and FAU). Differences in the activation entropy make a relatively small contribution ($\Delta\Delta S^{\ddagger}_{C-O,\ water-decalin}$ = ∼20−27 J mol^{-1} K^{-1}, or $T\Delta\Delta S^{\ddagger}_{C-O,\ water-decalin}$ = ∼8−12 kJ mol^{-1} at 403−433 K).

This lowering of the C−O scission TS relative to the monomer precursor state in decalin can be understood on the basis of the Hammond postulate, in view of a substantially more stable intermediate (i.e., surface alkoxide) that connects the C−O cleavage TS and the C−H cleavage TS (Scheme 3). In the case of MFI, the rate constant of the aqueous-phase dehydration[25] was similar to that of the monomer route ($k_{aqueous}$ = 0.03−0.18 vs $k_{M,\ decalin}$ = 0.05−0.15 s^{-1} at 413−433 K) in decalin. Surprisingly, however, a marked difference in the activation enthalpy was deduced for the two solvents (for the monomer-path: $\Delta\Delta H^{\ddagger}_{C-O,\ water-decalin}$ ∼60 kJ mol^{-1}), which was almost totally offset by entropic factors ($\Delta\Delta S^{\ddagger}_{C-O,\ water-decalin}$ ∼150 J mol^{-1} K^{-1}) at the studied range of temperature. In view of these different enthalpic and entropic components in the two solvents, the similar rate constants for MFI in decalin and in water are concluded to be coincidental.

Transition states for both C−O and C−H scissions typically occur late (i.e., resembling the products) along the reaction coordinate of alcohol dehydration[26,47,48,52] in aqueous- and gas-phase dehydration of alcohols catalyzed by protonic zeolites (e.g., much longer distances between the leaving water and the C_α atom than in the original alcohol, significant positive charges on the organic moiety). The zeolite framework or the pore confinement, however, does not seem to have a pronounced or systematic impact on the "lateness" of the

https://dx.doi.org/10.1021/acscatal.0c05674
ACS Catal. 2021, 11, 2879−2888

Scheme 3. An Illustration of the Energy Landscapes for Aqueous- and Decalin-Phase Dehydration of Cyclohexanol That Seeks to Explain, on the Basis of the Hammond Postulate That Links the Stability of Transition State (TS) to That of the Product State (in This Case, the Intermediate State between C−O and C−H Bond Cleavages), the Lower Measured Activation Barrier for C−O Cleavage in the Decalin-Phase Dehydration than in Aqueous-Phase Dehydration[a]

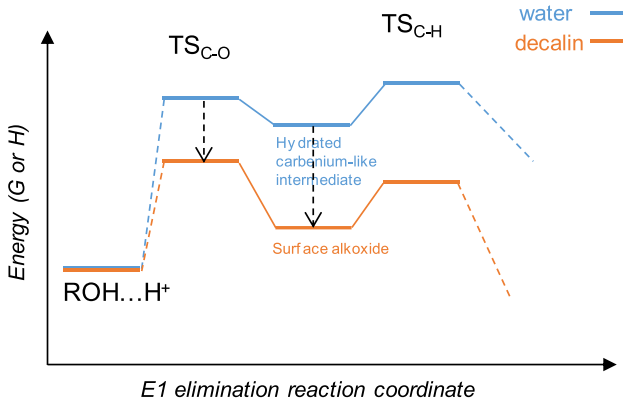

[a]Note that C−O TS and C−H TS lie at similar energies in the aqueous case[25]. The most populated initial states for C−O cleavage, shown as ROH. . .H$^+$, are different, being an adsorbed alcohol monomer at the zeolite proton in the decalin case, while being an ROH associated with hydronium ions in the water case; these two states are referenced to the same energy level in this scheme. Dashed lines are used to indicate that some steps (e.g., protonation) connecting two given states are omitted.

elimination or deprotonation TS according to theoretical calculations.[47] The high activation entropies observed for BEA and FAU in both water and decalin further suggest similar size of the TS relative to the ground state. Moreover, a very recent study from this group suggested that intraporous stabilization assumes greater significance over van der Waals stabilization provided by the larger pores of BEA for aqueous-phase alkanol dehydration.[53] Therefore, we hypothesize that the favorable enthalpic stabilization from the intraporous decalin and coadsorbed cyclohexanol lead to higher rate constants in decalin than water inside the confines of BEA and FAU. Presumably, this stabilization assumes lesser significance inside the narrower MFI pores.

3. CONCLUSIONS

On zeolites, the dehydration of cyclohexanol in decalin generally proceeds via E1-elimination routes mediated by alcohol monomer and dimer species. The only exception found in this study is the monomer route catalyzed by MFI, for which the low activation barrier and negative activation entropy point to a concerted elimination. The formation of cyclohexanol-cyclohexanol dimers at the Brønsted acid sites leads to a decrease in turnover frequency with increasing concentrations of cyclohexanol in decalin, most markedly in zeolites with large pores. However, at concentrations less than ∼1 M, the reaction rates are dominated by cyclohexanol monomers that exhibit 1 to 2 orders of magnitude higher rate constant than dimers.

Most likely, the framework-bound proton remains a predominant presence at relatively low conversions, though there is a finite possibility that hydronium ion clusters with a size substantially smaller than that in aqueous-phase catalysis may form in zeolite pores. These intraporous active sites lead to disparate kinetics of alkanol dehydration in decalin and in water: for large pore zeolites FAU and BEA, dehydration rates are 2−3 orders of magnitude higher in decalin than in aqueous solutions, while for MFI, the rates are similar in the two solvents.

In contrast to the aqueous-phase dehydration of cyclohexanol that exhibits a dominant degree of rate control by C−H bond cleavage (deprotonation of the cyclohexyl cation), C−O bond cleavage is more rate-controlling for the dehydration in decalin. The higher catalytic activity in apolar media is primarily driven by lower activation enthalpies than in aqueous solutions because of the greater stability of the alkoxy intermediate (compared with a less stable hydrated carbenium ion-like intermediate in the case of aqueous-phase dehydration) that forms upon C−O bond cleavage prior to subsequent deprotonation to olefin. The favorable enthalpic stabilization from the intraporous decalin and coadsorbed cyclohexanol molecules inside the confines of BEA and FAU lead to higher rate constants in decalin (than those in water), while this stabilization assumes lesser significance inside the narrower MFI pores, making Brønsted acid sites in FAU and BEA much more active than in MFI for the apolar-phase dehydration of cyclohexanol, an opposite trend to that observed in aqueous phase.

4. MATERIALS AND METHODS

4.1. Chemicals and Catalysts. Commercial zeolites were obtained in the H-form, activated (1 K min^{-1} to 723 K for 6 h) and stored in closed containers to prevent from contamination by volatile organics. Specifically, BEA (Si/Al = 75) was provided by Clariant AG, while MFI (CBV8014, Si/Al = 40) and FAU (CBV760;Si/Al$_{total}$ = 30, Si/Al$_F$ = 60) were obtained from Zeolyst International. Cyclohexanol (ReagentPlus, 99%), cyclohexene (99%), 1,3-dimethoxybenzene (99%), sodium sulfate (99%, anhydrous), dichloromethane (HPLC grade), cyclohexanol-d$_{12}$ (98−99 atom % D; containing a small but undetermined fraction of C$_6$D$_{10}$HOD) and sodium borodeuteride (98 atom % D, 90% (CP)) were purchased from Sigma−Aldrich and used as received without further purification. Water (H$_2$O, resistivity 18.2 MΩ·cm) was taken from an ultrapure water dispenser system.

4.2. Preparation of 1-D-Cyclohexanol. Cyclohexanone (3.8 g, 38.5 mmol) was mixed with 100 mL of water in a 250

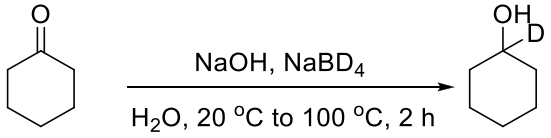

mL round-bottom flask. Then 0.775 g (19.4 mmol) of NaOH pellets was added to the solution under continuous stirring at room temperature. After NaOH dissolved, 0.82 g (17.6 mmol) of NaBD$_4$ was slowly added to the flask. After 5 min, the solution was heated and refluxed for 2 h with stirring. After it was cooled to room temperature, the solution was extracted twice with diethyl ether (100 mL × 2). The combined ether solution was dried over anhydrous Na$_2$SO$_4$. Finally, the product 1-D-cyclohexanol was obtained after distillation in an oil bath, with its purity checked by NMR.

https://dx.doi.org/10.1021/acscatal.0c05674
ACS Catal. 2021, 11, 2879−2888

4.3. Kinetic Measurements. The dehydration reactions were performed in a 300 mL Hastelloy Parr reactor, a gradientless batch reactor. Preliminary tests showed that the zeolite samples (protected from contaminants) could be used off-the-shelf without reactivation procedures. For reactions catalyzed by solid acids, the external diffusion limitation (mass transport of the dissolved reactants from the liquid bulk to the outer surface of the catalyst particles) was ruled out in preliminary experiments by varying the stirring speed (400−700 rpm) and catalyst loading (10−100 mg). In a typical experiment, 2.4 g of cyclohexanol in 78 mL of decalin solution (0.3 M) with 100 mg of zeolite were loaded in the reactor. The sealed reactor was then pressurized with 40 bar of H_2 at room temperature and heated to the set temperature. During heating, the stirring rate was typically less than 100 rpm. The stirring rate was adjusted to 700 rpm once the set temperature was reached. The reaction time was based on the point when the set temperature was reached (typically 30 min). H_2 and its pressure had no effect on the dehydration reaction and was found to be totally replaceable with N_2, except for an observation of a faster heating profile under high pressure H_2 while under low stirring (<100 rpm). At the end of a reaction, the reactor was cooled with an ice/water mixture to at least 278 K. The reaction mixture was isolated by centrifugation, and an aliquot of the solution was analyzed on an Agilent 7890A GC equipped with a HP-5 ms 25m × 0.25 mm (i.d.) column and a flame ionization detector. 1,3-Dimethoxybenzene was used as the standard for quantification (added to the liquid after opening the reactor and extracted together).

By measuring the composition of the reaction mixture at different time points and dividing the moles of olefin (cyclohexene) formed by the time elapsed and the mass of catalyst (or the BAS concentration), the rate of olefin formation was obtained (on a mass basis or site basis). As discussed in Section 2.2, the rate of dehydration decreases with increasing concentration of cyclohexanol, and thus, this rate assessment protocol provides an average rate value within the studied conversion range (albeit relatively low) and somewhat underestimates the true initial rates at the starting alcohol concentration.

4.4. H/D KIE Measurements. For H/D KIE measurements, 0.025 or 0.1 M 1-D-cyclohexanol or cyclohexanol-d_{12} in decalin solution with 10−100 mg of zeolite were loaded in the reactor. The sealed reactor was then pressurized with 40 bar of H_2 at room temperature and heated to the set temperature while being stirred vigorously (700 rpm). The reaction time was based on the point when the set temperature was reached (ca. 30 min after heating was started). At the end of a reaction, the reactor was cooled with an ice/water mixture to at least 278 K. The reaction mixture was isolated by centrifugation, and an aliquot of the solution was analyzed by GC, using 1,3-dimethoxybenzene as the standard for quantification (added to the liquid after opening the reactor).

4.5. Liquid-Phase Adsorption and Calorimetry. Heat of adsorption of cyclohexanol from decalin solutions onto zeolites was determined by liquid calorimetry using a Setaram Calvet C80 calorimeter. Reversal mixing cells were used to separate the adsorptive from the adsorbent. The lower compartment was loaded with 0.03 g of zeolite (m) immersed in 1.0 mL of decalin. The upper compartment was loaded with 1.0 mL of the desired cyclohexanol solution resulting in a total volume (V) of 2 mL with a concentration c_0. The reference cell was loaded with identical compositions, without zeolite. Uptake (q) was determined using GC by measuring the difference in alcohol concentration between the starting solution and the solution at equilibrium (alcohol concentration c_e): $q = V(c_0-c_e)m^{-1}$. Adsorption isotherms were obtained by immersing 100 mg of zeolite in a cyclohexanol-decalin solution of a defined alcohol concentration for at least 24 h.

4.6. Infrared (IR) Spectroscopy of Adsorbed Pyridine. IR spectra of adsorbed pyridine were recorded with a Perkin−Elmer 2000 spectrometer at a resolution of 4 cm^{-1}. The catalyst samples were prepared as self−supporting wafers and activated in vacuum ($p = 10^{-6}$ mbar) at 723 K for 1 h at a heating rate of 10 K min^{-1}. After it was cooled to 423 K, the sample was equilibrated with 0.1 mbar pyridine for 0.5 h followed by outgassing for 1 h and the acquisition of the spectrum. Finally, desorption program (up to 723 K with 10 K min^{-1} and 0.5 h at 723 K) was initiated and the spectra were recorded until equilibrium was achieved. The concentrations of BAS and LAS are quantified using the integrated areas of peaks at 1540 and 1450 cm^{-1}, respectively. The number of pyridine molecules retained after evacuation at 423 and 723 K were used to determine the concentrations of total and strong acid sites, respectively. For quantification, molar integral extinction coefficients of 0.73 and 0.96 cm μmol^{-1} were used for BAS and LAS, respectively.[54,55]

■ ASSOCIATED CONTENT

Supporting Information

The Supporting Information is available free of charge at https://pubs.acs.org/doi/10.1021/acscatal.0c05674.

Physicochemical properties of parent zeolites, additional rate data, results of ^2H NMR experiments and isotopic tracer experiments, derivations of rate equations, and additional discussion on fitting results, the rate-determining step and chemical state of acid sites (PDF)

■ AUTHOR INFORMATION

Corresponding Authors

Hui Shi − *Department of Chemistry and Catalysis Research Center, Technische Universität München, 85748 Garching, Germany;* orcid.org/0000-0003-1180-7443; Email: shihui@yzu.edu.cn

Johannes A. Lercher − *Institute for Integrated Catalysis, Pacific Northwest National Laboratory, Richland, Washington 99352, United States; Department of Chemistry and Catalysis Research Center, Technische Universität München, 85748 Garching, Germany;* orcid.org/0000-0002-2495-1404; Email: Johannes.lercher@pnnl.gov

Authors

Feng Chen − *Institute for Integrated Catalysis, Pacific Northwest National Laboratory, Richland, Washington 99352, United States;* orcid.org/0000-0002-5227-6119

Manish Shetty − *Institute for Integrated Catalysis, Pacific Northwest National Laboratory, Richland, Washington 99352, United States;* orcid.org/0000-0002-8611-7415

Meng Wang − *Institute for Integrated Catalysis, Pacific Northwest National Laboratory, Richland, Washington 99352, United States;* orcid.org/0000-0002-3380-3534

https://dx.doi.org/10.1021/acscatal.0c05674
ACS Catal. 2021, 11, 2879−2888

Yuanshuai Liu − *Department of Chemistry and Catalysis Research Center, Technische Universität München, 85748 Garching, Germany*

Donald M. Camaioni − *Institute for Integrated Catalysis, Pacific Northwest National Laboratory, Richland, Washington 99352, United States;* orcid.org/0000-0002-2213-0960

Oliver Y. Gutiérrez − *Institute for Integrated Catalysis, Pacific Northwest National Laboratory, Richland, Washington 99352, United States;* orcid.org/0000-0001-9163-4786

Complete contact information is available at: https://pubs.acs.org/10.1021/acscatal.0c05674

Notes

The authors declare no competing financial interest.

■ ACKNOWLEDGMENTS

This work is supported by the U.S. Department of Energy (DOE), Office of Science, Office of Basic Energy Sciences (BES), Division of Chemical Sciences, Geosciences and Biosciences (Transdisciplinary Approaches to Realize Novel Catalytic Pathways to Energy Carriers, FWP 47319). Portions of the experiments were performed at the William R. Environmental Molecular Science Laboratory (EMSL), a national scientific user facility sponsored by the DOE Office of Biological and Environmental Research located at Pacific Northwest National Laboratory (PNNL). PNNL is a multi-program national laboratory operated for DOE by Battelle.

■ REFERENCES

(1) Corma, A.; Iborra, S.; Velty, A. Chemical Routes for the Transformation of Biomass into Chemicals. *Chem. Rev.* **2007**, *107*, 2411−2502.

(2) Straathof, A. J. J. Transformation of Biomass into Commodity Chemicals Using Enzymes or Cells. *Chem. Rev.* **2014**, *114*, 1871−1908.

(3) Navarro, R. M.; Peña, M. A.; Fierro, J. L. G. Hydrogen Production Reactions from Carbon Feedstocks: Fossil Fuels and Biomass. *Chem. Rev.* **2007**, *107*, 3952−3991.

(4) Huber, G. W.; Iborra, S.; Corma, A. Synthesis of Transportation Fuels from Biomass: Chemistry, Catalysts, and Engineering. *Chem. Rev.* **2006**, *106*, 4044−4098.

(5) Sudarsanam, P.; Zhong, R.; Van den Bosch, S.; Coman, S. M.; Parvulescu, V. I.; Sels, B. F. Functionalised heterogeneous catalysts for sustainable biomass valorisation. *Chem. Soc. Rev.* **2018**, *47*, 8349−8402.

(6) Ennaert, T.; Van Aelst, J.; Dijkmans, J.; De Clercq, R.; Schutyser, W.; Dusselier, M.; Verboekend, D.; Sels, B. F. Potential and challenges of zeolite chemistry in the catalytic conversion of biomass. *Chem. Soc. Rev.* **2016**, *45*, 584−611.

(7) Lanzafame, P.; Centi, G.; Perathoner, S. Catalysis for biomass and CO2 use through solar energy: opening new scenarios for a sustainable and low-carbon chemical production. *Chem. Soc. Rev.* **2014**, *43*, 7562−7580.

(8) Alonso, D. M.; Wettstein, S. G.; Dumesic, J. A. Bimetallic catalysts for upgrading of biomass to fuels and chemicals. *Chem. Soc. Rev.* **2012**, *41*, 8075−8098.

(9) Gallezot, P. Conversion of biomass to selected chemical products. *Chem. Soc. Rev.* **2012**, *41*, 1538−1558.

(10) Zhou, C.-H.; Xia, X.; Lin, C.-X.; Tong, D.-S.; Beltramini, J. Catalytic conversion of lignocellulosic biomass to fine chemicals and fuels. *Chem. Soc. Rev.* **2011**, *40*, 5588−5617.

(11) Serrano-Ruiz, J. C.; Luque, R.; Sepúlveda-Escribano, A. Transformations of biomass-derived platform molecules: from high added-value chemicals to fuelsvia aqueous-phase processing. *Chem. Soc. Rev.* **2011**, *40*, 5266−5281.

(12) Deshlahra, P.; Carr, R. T.; Chai, S.-H.; Iglesia, E. Mechanistic Details and Reactivity Descriptors in Oxidation and Acid Catalysis of Methanol. *ACS Catal.* **2015**, *5*, 666−682.

(13) Macht, J.; Carr, R. T.; Iglesia, E. Consequences of Acid Strength for Isomerization and Elimination Catalysis on Solid Acids. *J. Am. Chem. Soc.* **2009**, *131*, 6554−6565.

(14) Jones, A. J.; Zones, S. I.; Iglesia, E. Implications of Transition State Confinement within Small Voids for Acid Catalysis. *J. Phys. Chem. C* **2014**, *118*, 17787−17800.

(15) Jones, A. J.; Carr, R. T.; Zones, S. I.; Iglesia, E. Acid strength and solvation in catalysis by MFI zeolites and effects of the identity, concentration and location of framework heteroatoms. *J. Catal.* **2014**, *312*, 58−68.

(16) Deshlahra, P.; Carr, R. T.; Iglesia, E. Ionic and Covalent Stabilization of Intermediates and Transition States in Catalysis by Solid Acids. *J. Am. Chem. Soc.* **2014**, *136*, 15229−15247.

(17) Simonetti, D. A.; Carr, R. T.; Iglesia, E. Acid strength and solvation effects on methylation, hydride transfer, and isomerization rates during catalytic homologation of C1 species. *J. Catal.* **2012**, *285*, 19−30.

(18) Bregante, D. T.; Johnson, A. M.; Patel, A. Y.; Ayla, E. Z.; Cordon, M. J.; Bukowski, B. C.; Greeley, J.; Gounder, R.; Flaherty, D. W. Cooperative Effects between Hydrophilic Pores and Solvents: Catalytic Consequences of Hydrogen Bonding on Alkene Epoxidation in Zeolites. *J. Am. Chem. Soc.* **2019**, *141*, 7302−7319.

(19) Di Iorio, J. R.; Johnson, B. A.; Román-Leshkov, Y. Ordered Hydrogen-Bonded Alcohol Networks Confined in Lewis Acid Zeolites Accelerate Transfer Hydrogenation Turnover Rates. *J. Am. Chem. Soc.* **2020**, *142*, 19379−19392.

(20) Cordon, M. J.; Harris, J. W.; Vega-Vila, J. C.; Bates, J. S.; Kaur, S.; Gupta, M.; Witzke, M. E.; Wegener, E. C.; Miller, J. T.; Flaherty, D. W.; Hibbitts, D. D.; Gounder, R. Dominant Role of Entropy in Stabilizing Sugar Isomerization Transition States within Hydrophobic Zeolite Pores. *J. Am. Chem. Soc.* **2018**, *140*, 14244−14266.

(21) Mellmer, M. A.; Sanpitakseree, C.; Demir, B.; Bai, P.; Ma, K.; Neurock, M.; Dumesic, J. A. Solvent-enabled control of reactivity for liquid-phase reactions of biomass-derived compounds. *Nature Catal.* **2018**, *1*, 199−207.

(22) Walker, T. W.; Chew, A. K.; Li, H.; Demir, B.; Zhang, Z. C.; Huber, G. W.; Van Lehn, R. C.; Dumesic, J. A. Universal kinetic solvent effects in acid-catalyzed reactions of biomass-derived oxygenates. *Energy Environ. Sci.* **2018**, *11*, 617−628.

(23) Mellmer, M. A.; Sener, C.; Gallo, J. M. R.; Luterbacher, J. S.; Alonso, D. M.; Dumesic, J. A. Solvent Effects in Acid-Catalyzed Biomass Conversion Reactions. *Angew. Chem., Int. Ed.* **2014**, *53*, 11872−11875.

(24) Wang, M.; Jaegers, N. R.; Lee, M.-S.; Wan, C.; Hu, J. Z.; Shi, H.; Mei, D.; Burton, S. D.; Camaioni, D. M.; Gutiérrez, O. Y.; Glezakou, V.-A.; Rousseau, R.; Wang, Y.; Lercher, J. A. Genesis and Stability of Hydronium Ions in Zeolite Channels. *J. Am. Chem. Soc.* **2019**, *141*, 3444−3455.

(25) Shi, H.; Eckstein, S.; Vjunov, A.; Camaioni, D. M.; Lercher, J. A. Tailoring nanoscopic confines to maximize catalytic activity of hydronium ions. *Nat. Commun.* **2017**, *8*, 15442.

(26) Liu, Y.; Vjunov, A.; Shi, H.; Eckstein, S.; Camaioni, D. M.; Mei, D.; Barath, E.; Lercher, J. A. Enhancing the catalytic activity of hydronium ions through constrained environments. *Nat. Commun.* **2017**, *8*, 14113.

(27) Kunkes, E. L.; Simonetti, D. A.; West, R. M.; Serrano-Ruiz, J. C.; Gärtner, C. A.; Dumesic, J. A. Catalytic Conversion of Biomass to Monofunctional Hydrocarbons and Targeted Liquid-Fuel Classes. *Science* **2008**, *322*, 417−421.

(28) Saidi, M.; Samimi, F.; Karimipourfard, D.; Nimmanwudipong, T.; Gates, B. C.; Rahimpour, M. R. Upgrading of lignin-derived bio-oils by catalytic hydrodeoxygenation. *Energy Environ. Sci.* **2014**, *7*, 103−129.

(29) Lohr, T. L.; Li, Z.; Marks, T. J. Thermodynamic Strategies for C-O Bond Formation and Cleavage via Tandem Catalysis. *Acc. Chem. Res.* **2016**, *49*, 824−834.
(30) Robinson, A. M.; Hensley, J. E.; Medlin, J. W. Bifunctional Catalysts for Upgrading of Biomass-Derived Oxygenates: A Review. *ACS Catal.* **2016**, *6*, 5026−5043.
(31) Sun, Z.; Fridrich, B.; de Santi, A.; Elangovan, S.; Barta, K. Bright Side of Lignin Depolymerization: Toward New Platform Chemicals. *Chem. Rev.* **2018**, *118*, 614−678.
(32) Lin, Z.; Chen, R.; Qu, Z.; Chen, J. G. Hydrodeoxygenation of biomass-derived oxygenates over metal carbides: from model surfaces to powder catalysts. *Green Chem.* **2018**, *20*, 2679−2696.
(33) Remy, R.; Bochet, C. G. Arene-Alkene Cycloaddition. *Chem. Rev.* **2016**, *116*, 9816−9849.
(34) Dong, Z.; Ren, Z.; Thompson, S. J.; Xu, Y.; Dong, G. Transition-Metal-Catalyzed C-H Alkylation Using Alkenes. *Chem. Rev.* **2017**, *117*, 9333−9403.
(35) Kress, S.; Blechert, S. Asymmetric catalysts for stereocontrolled olefin metathesis reactions. *Chem. Soc. Rev.* **2012**, *41*, 4389−4408.
(36) Hughes, D.; Wheeler, P.; Ene, D. Olefin Metathesis in Drug Discovery and Development—Examples from Recent Patent Literature. *Org. Process Res. Dev.* **2017**, *21*, 1938−1962.
(37) Zhao, Z.; Shi, H.; Wan, C.; Hu, M. Y.; Liu, Y.; Mei, D.; Camaioni, D. M.; Hu, J. Z.; Lercher, J. A. Mechanism of Phenol Alkylation in Zeolite H-BEA Using In Situ Solid-State NMR Spectroscopy. *J. Am. Chem. Soc.* **2017**, *139*, 9178−9185.
(38) Liu, Y.; Baráth, E.; Shi, H.; Hu, J.; Camaioni, D. M.; Lercher, J. A. Solvent-determined mechanistic pathways in zeolite-H-BEA-catalysed phenol alkylation. *Nature Catal.* **2018**, *1*, 141−147.
(39) Eckstein, S.; Hintermeier, P. H.; Zhao, R.; Baráth, E.; Shi, H.; Liu, Y.; Lercher, J. A. Influence of Hydronium Ions in Zeolites on Sorption. *Angew. Chem., Int. Ed.* **2019**, *58*, 3450−3455.
(40) Chiang, H.; Bhan, A. Catalytic consequences of hydroxyl group location on the rate and mechanism of parallel dehydration reactions of ethanol over acidic zeolites. *J. Catal.* **2010**, *271*, 251−261.
(41) Zhi, Y.; Shi, H.; Mu, L.; Liu, Y.; Mei, D.; Camaioni, D. M.; Lercher, J. A. Dehydration Pathways of 1-Propanol on HZSM-5 in the Presence and Absence of Water. *J. Am. Chem. Soc.* **2015**, *137*, 15781−15794.
(42) Lee, K. Y.; Arai, T.; Nakata, S.; Asaoka, S.; Okuhara, T.; Misono, M. Catalysis by heteropoly compounds. 20. An NMR study of ethanol dehydration in the pseudoliquid phase of 12-tungstophosphoric acid. *J. Am. Chem. Soc.* **1992**, *114*, 2836−2842.
(43) Knaeble, W.; Iglesia, E. Kinetic and Theoretical Insights into the Mechanism of Alkanol Dehydration on Solid Brønsted Acid Catalysts. *J. Phys. Chem. C* **2016**, *120*, 3371−3389.
(44) Macht, J.; Janik, M. J.; Neurock, M.; Iglesia, E. Catalytic Consequences of Composition in Polyoxometalate Clusters with Keggin Structure. *Angew. Chem., Int. Ed.* **2007**, *46*, 7864−7868.
(45) Macht, J.; Janik, M. J.; Neurock, M.; Iglesia, E. Mechanistic Consequences of Composition in Acid Catalysis by Polyoxometalate Keggin Clusters. *J. Am. Chem. Soc.* **2008**, *130*, 10369−10379.
(46) John, M.; Alexopoulos, K.; Reyniers, M.-F.; Marin, G. B. Mechanistic insights into the formation of butene isomers from 1-butanol in H-ZSM-5: DFT based microkinetic modelling. *Catal. Sci. Technol.* **2017**, *7*, 1055−1072.
(47) John, M.; Alexopoulos, K.; Reyniers, M.-F.; Marin, G. B. First-Principles Kinetic Study on the Effect of the Zeolite Framework on 1-Butanol Dehydration. *ACS Catal.* **2016**, *6*, 4081−4094.
(48) John, M.; Alexopoulos, K.; Reyniers, M.-F.; Marin, G. B. Reaction path analysis for 1-butanol dehydration in H-ZSM-5 zeolite: Ab initio and microkinetic modeling. *J. Catal.* **2015**, *330*, 28−45.
(49) Campbell, C. T. Future Directions and Industrial Perspectives Micro- and macro-kinetics: Their relationship in heterogeneous catalysis. *Top. Catal.* **1994**, *1*, 353−366.
(50) Stegelmann, C.; Andreasen, A.; Campbell, C. T. Degree of Rate Control: How Much the Energies of Intermediates and Transition States Control Rates. *J. Am. Chem. Soc.* **2009**, *131*, 8077−8082.
(51) Campbell, C. T. The Degree of Rate Control: A Powerful Tool for Catalysis Research. *ACS Catal.* **2017**, *7*, 2770−2779.
(52) Mei, D.; Lercher, J. A. Mechanistic insights into aqueous phase propanol dehydration in H-ZSM-5 zeolite. *AIChE J.* **2017**, *63*, 172−184.
(53) Shetty, M.; Wang, H.; Chen, F.; Jaegers, N. R.; Liu, Y.; Camaioni, D. M.; Gutierrez, O. Y.; Lercher, J. Directing the rate-enhancement for hydronium ion catalyzed dehydration via organization of alkanols in nanoscopic confinements. *Angew. Chem., Int. Ed.* **2020**, *60*, 2304−2311.
(54) Lercher, J. A.; Gründling, C.; Eder-Mirth, G. Infrared studies of the surface acidity of oxides and zeolites using adsorbed probe molecules. *Catal. Today* **1996**, *27*, 353−376.
(55) Vimont, A.; Thibault-Starzyk, F.; Daturi, M. Analysing and understanding the active site by IR spectroscopy. *Chem. Soc. Rev.* **2010**, *39*, 4928−4950.

https://dx.doi.org/10.1021/acscatal.0c05674
ACS Catal. 2021, 11, 2879−2888